Mon. Not. R. Astron. Soc. **000**, 000–000 (0000) Printed 27 February 2013 (MN LATEX style file v2.2)

Jet launching from accretion discs in the local approximation

Gordon I. Ogilvie
Department of Applied Mathematics and Theoretical Physics, University of Cambridge, Centre for Mathematical Sciences, Wilberforce Road, Cambridge CB3 0WA

27 February 2013

ABSTRACT

The acceleration of an outflow along inclined magnetic field lines emanating from an accretion disc can be studied in the local approximation, as employed in the computational model known as the shearing box. By including the slow magnetosonic point within the computational domain, the rate of mass loss in the outflow can be calculated. The accretion rates of mass and magnetic flux can also be determined, although some effects of cylindrical geometry are omitted. We formulate a simple model for the study of this problem and present the results of one-dimensional numerical simulations and supporting calculations. Quasi-steady solutions are obtained for relatively strong poloidal magnetic fields for which the magnetorotational instability is suppressed. In this regime the rate of mass loss decreases extremely rapidly with increasing field strength, or with decreasing surface density or temperature. If the poloidal magnetic field in an accretion disc can locally achieve an appropriate strength and inclination then a rapid burst of ejection may occur. For weaker fields it may be possible to study the launching process in parallel with the magnetorotational instability, but this will require three-dimensional simulations.

Key words: accretion, accretion discs – ISM: jets and outflows – magnetic fields – MHD

1 INTRODUCTION

In a well known paper, Blandford & Payne (1982) presented a mechanism by which jets or winds can be launched from accretion discs. Consider a disc that is threaded by a poloidal magnetic field and is sufficiently ionized for ideal magnetohydrodynamics (MHD) to be a good approximation. Above the surface of the disc, where the magnetic field is dynamically dominant, gas tends to rotate with the same angular velocity as the part of the disc to which is magnetically connected; its motion in the meridional plane also tends to be parallel to the magnetic field. Above a thin Keplerian disc, the net acceleration of gas parallel to the field is directed away from the disc if the poloidal field is inclined at more than 30° to the vertical, when both the centrifugal and gravitational forces are taken into account.

Fig. 1, based on Fig. 1 of Blandford & Payne (1982), illustrates the effective potential experienced by gas that is forced to corotate with the angular velocity of a Keplerian orbit of radius r_0 in the plane $z = 0$. Near the saddle point of the effective potential at this same location, acceleration away from the disc can occur if the inclination exceeds 30° either to the left or to the right. Indeed, the picture is symmetrical near the saddle point. Globally, however, only flows that are directed away from the rotation axis are suitable for launching jets.

2 LOCAL APPROXIMATION

2.1 Introduction

The shearing sheet (Fig. 2; Goldreich & Lynden-Bell 1965) is a widely adopted local model of an astrophysical disc. The sheet is centred on a reference point that follows a circular orbit around the central mass, and the frame rotates with the angular velocity Ω of this orbit. The differential rotation of the disc is represented locally as a uniform parallel shear flow in the rotating frame. The local approximation has two symmetries not present in the global system: it is invariant under translation in the x direction (allowing for a Galilean transformation in the y direction to correct for the velocity shift) and under rotation by 180° about the z axis. The latter symmetry might appear to make the shearing sheet unsuitable for studying jet launching, because it fails to distinguish between radially inward and outward directions; however, as noted above, this symmetry is indeed present in the problem of Blandford & Payne (1982) close to the disc.

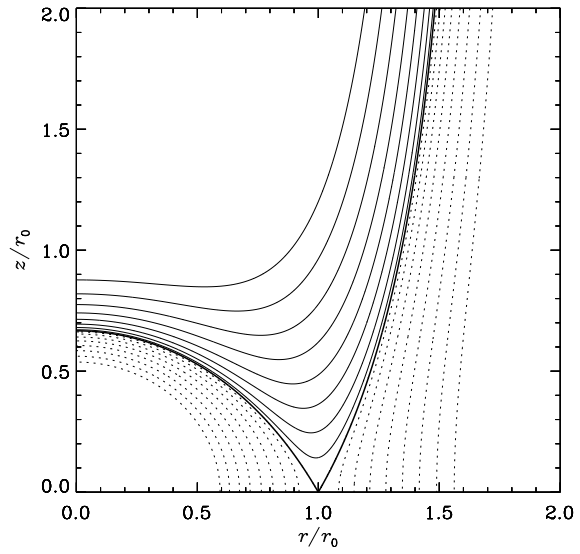

Figure 1. Contours of the effective potential experienced by matter that is forced to rotate with the Keplerian angular velocity at radius r_0. The contour values are unequally spaced. Dotted contours correspond to values lower than that of the saddle point.

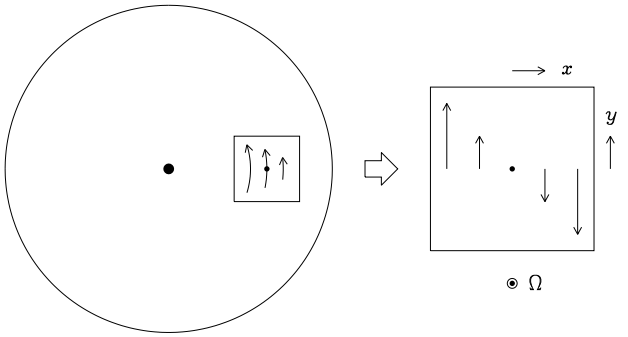

Figure 2. The shearing sheet, or local approximation. Coordinates x, y and z are measured in the radial, azimuthal and vertical directions.

For simplicity, we assume in this paper that the disc orbits in a Newtonian potential, giving rise to Keplerian rotation in the absence of other radial forces, and that the gas is isothermal, its pressure and density being related by $p = c_{\rm s}^2\rho$, with a uniform isothermal sound speed $c_{\rm s}$. The gas satisfies the equation of motion,

$$\rho\left(\frac{\partial \boldsymbol{u}}{\partial t} + \boldsymbol{u}\cdot\boldsymbol{\nabla}\boldsymbol{u} + 2\Omega\,\boldsymbol{e}_z\times\boldsymbol{u}\right) = -\rho\boldsymbol{\nabla}\Phi - \boldsymbol{\nabla}p + \boldsymbol{J}\times\boldsymbol{B} + \boldsymbol{\nabla}\cdot\mathbf{T}, \tag{1}$$

the equation of mass conservation,

$$\frac{\partial\rho}{\partial t} + \boldsymbol{\nabla}\cdot(\rho\boldsymbol{u}) = 0, \tag{2}$$

the induction equation,

$$\frac{\partial \boldsymbol{B}}{\partial t} = \boldsymbol{\nabla}\times(\boldsymbol{u}\times\boldsymbol{B} - \eta\boldsymbol{\nabla}\times\boldsymbol{B}), \tag{3}$$

and the solenoidal condition

$$\boldsymbol{\nabla}\cdot\boldsymbol{B} = 0. \tag{4}$$

Here $\Phi = \frac{1}{2}\Omega^2(z^2 - 3x^2)$ is the effective (tidal) potential in the local approximation, which comes from expanding the sum of the gravitational and centrifugal potentials to second order in the distance from the centre of the sheet. Also $\boldsymbol{J} = \mu_0^{-1}\boldsymbol{\nabla}\times\boldsymbol{B}$ is the electric current density and $T_{ij} = \rho\nu(u_{i,j}+u_{j,i}) + \rho(\nu_{\rm b} - \frac{2}{3}\nu)u_{k,k}\delta_{ij}$ is the viscous stress tensor. We assume that the kinematic shear and bulk viscosities ν and $\nu_{\rm b}$ and the magnetic diffusivity η are uniform.

The hyperbolic contours of Φ in the xz plane agree with those of the effective potential plotted in Fig. 1 close to the saddle point and reproduce the critical inclination of 30°. The reason for this is of course that Φ is the effective potential experienced by matter that is forced to rotate with the Keplerian angular velocity Ω of the reference point.

The basic state of the shearing sheet in the absence of magnetic fields consists of the Keplerian shear flow $\boldsymbol{u} = -\frac{3}{2}\Omega x\,\boldsymbol{e}_y$ together with the hydrostatic density distribution $\rho = \rho_0\exp(-z^2/2H^2)$, where ρ_0 is a constant and $H = c_{\rm s}/\Omega$ is the isothermal scaleheight. The departure from the basic Keplerian flow is denoted by $\boldsymbol{v} = \boldsymbol{u} + \frac{3}{2}\Omega x\,\boldsymbol{e}_y$.

This system of equations can be solved numerically in a finite shearing box (e.g. Hawley, Gammie & Balbus 1995), in which case shearing-periodic horizontal boundary conditions apply to the solution (to $\boldsymbol{v}$ rather than $\boldsymbol{u}$), while various vertical boundary conditions are permissible. The shearing box has been widely employed in treatments of the magnetorotational instability (MRI) (Balbus & Hawley 1998, and references therein), but has not been used for studies of jet launching. [The recent work of Suzuki & Inutsuka (2009) and Suzuki, Muto & Inutsuka (2010) finds mass loss from the computational domain but does not consider the systematically inclined fields relevant for the mechanism of Blandford & Payne (1982).]

2.2 Vertical boundary conditions

For any choice of vertical boundary conditions at $z = \pm Z$, and with shearing-periodic horizontal boundary conditions, the horizontal average over the box of B_z is independent of z and t, and is determined by the initial conditions. Within the local approximation, the type of poloidal magnetic field configuration that is favourable for jet launching consists of a uniform vertical field B_z together with a radial field B_x that is odd in z and tends to a non-zero constant at large z; this represents a field that is straight, inclined, current-free and therefore force-free in the low-density gas at large $|z|$ and bends symmetrically as it passes through the disc, producing a radial Lorentz force through the azimuthal current J_y (Fig. 3).

In this type of study, where a thin disc is to be connected to a jet, the question arises of which quantities are determined by the disc and which by the jet (see Ogilvie & Livio 2001, and references therein). Efficient outflows pass through a slow magnetosonic point not far above the surface of the disc and through an Alfvén point much higher up (Spruit 1996). It is convenient to think of matching the disc to the jet a small distance above the slow magnetosonic point, in a region where the magnetic field is predominantly poloidal and approximately force-free. Local studies of the disc can

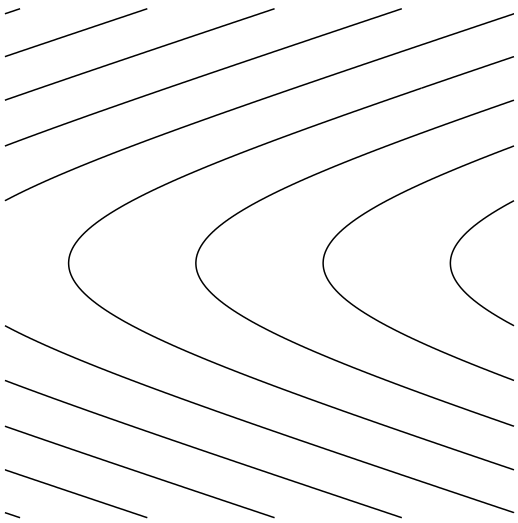

Figure 3. Geometry of the poloidal magnetic field in the (x, z) plane that is favourable for jet launching in the local approximation. The field lines could equally well bend the other way.

focus on the dynamics of the disc and the passage of the outflow through the slow point, which determines the rate of mass loss. However, the rate of angular momentum loss, and therefore the magnetic torque on the disc, are determined by the passage of the outflow through the Alfvén point, which usually lies outside the domain of the local approximation. Since the magnetic torque is proportional to the azimuthal magnetic field, the value of B_y in the matching region is determined by the jet region, not the disc region. Given the distribution of poloidal magnetic flux on the midplane of the disc, the global shape of the poloidal magnetic field is also determined by the jet region. It is therefore appropriate to impose on the local disc the value of B_z and the values of B_x and B_y in the matching region. This can be done by a novel type of boundary condition in which the horizontal components of the magnetic field are specified at the vertical boundaries, with equal and opposite values at the top and bottom because of the desired symmetry. At the same time, the vertical boundary conditions should leave the density and the velocity free to evolve according to the dynamics of the outflow that develops.

2.3 Evolution of the horizontal momentum

Let angle brackets denote a horizontal average over the box. Then, by rewriting the horizontal components of the equation of motion in conservative form and integrating over the box, we obtain

$$\partial_t \int_{-Z}^{Z} \langle \rho v_x \rangle \, \mathrm{d}z - 2\Omega \int_{-Z}^{Z} \langle \rho v_y \rangle \, \mathrm{d}z = \left[\left\langle \frac{B_x B_z}{\mu_0} - \rho v_x v_z + T_{xz} \right\rangle \right]_{-Z}^{Z}, \tag{5}$$

$$\partial_t \int_{-Z}^{Z} \langle \rho v_y \rangle \, \mathrm{d}z + \frac{1}{2}\Omega \int_{-Z}^{Z} \langle \rho v_x \rangle \, \mathrm{d}z = \left[\left\langle \frac{B_y B_z}{\mu_0} - \rho v_y v_z + T_{yz} \right\rangle \right]_{-Z}^{Z}. \tag{6}$$

In most shearing-box simulations the right-hand sides of these equations are negligible or zero, with the result that the mean horizontal momentum of the box executes an epicyclic oscillation of constant amplitude, which can be made to vanish by a suitable choice of initial conditions. Here, however, we wish to impose non-vanishing time-independent magnetic stresses at the vertical boundaries. These provide source terms for the epicyclic oscillation. If the initial conditions are chosen carefully, a non-oscillatory solution is possible, in which the xz stress is matched by a mean flow in the y direction and the yz stress by a mean flow in the x direction. The first represents a departure from Keplerian rotation induced by the radial Lorentz force of a poloidal magnetic field that bends through the disc, while the second represents an accretion flow driven by an imposed magnetic torque. For most initial conditions, however, a free epicyclic oscillation of constant amplitude and phase will be superimposed on this non-oscillatory solution. (In fact, depending on the way that mass loss from a finite computational domain is treated, the amplitude may *not* be constant, as is discussed below.)

3 HORIZONTALLY UNIFORM SOLUTIONS

We do not attempt the numerical solution of this system in multiple dimensions in this paper. Indeed, simulations of the MRI including both vertical gravity and a net vertical magnetic field present serious numerical and interpretative difficulties (Miller & Stone 2000; S. Fromang, private communication; G. Lesur, private communication; J. M. Stone, private communication). For the remainder of this paper we focus on horizontally uniform solutions that depend only on z and t. These are admissible because of the horizontal translational symmetry of the local approximation. Then we have

$$\rho \left(\frac{\partial v_x}{\partial t} + v_z \frac{\partial v_x}{\partial z} - 2\Omega v_y \right) = J_y B_z + \frac{\partial}{\partial z} \left(\rho \nu \frac{\partial v_x}{\partial z} \right), \tag{7}$$

$$\rho \left(\frac{\partial v_y}{\partial t} + v_z \frac{\partial v_y}{\partial z} + \frac{1}{2}\Omega v_x \right) = -J_x B_z + \frac{\partial}{\partial z} \left(\rho \nu \frac{\partial v_y}{\partial z} \right), \tag{8}$$

$$\rho \left(\frac{\partial v_z}{\partial t} + v_z \frac{\partial v_z}{\partial z} \right) = -\rho \Omega^2 z - \frac{\partial p}{\partial z} + J_x B_y - J_y B_x + \frac{\partial}{\partial z} \left[\rho (\nu_\mathrm{b} + \tfrac{4}{3}\nu) \frac{\partial v_z}{\partial z} \right], \tag{9}$$

$$\frac{\partial \rho}{\partial t} + \frac{\partial}{\partial z}(\rho v_z) = 0, \tag{10}$$

$$\frac{\partial B_x}{\partial t} = \frac{\partial E_y}{\partial z}, \tag{11}$$

$$\frac{\partial B_y}{\partial t} = -\frac{3}{2}\Omega B_x - \frac{\partial E_x}{\partial z}, \tag{12}$$

$$\frac{\partial B_z}{\partial t} = 0, \tag{13}$$

$$\frac{\partial B_z}{\partial z} = 0, \tag{14}$$

with

$$E_x = v_z B_y - v_y B_z + \eta J_x, \tag{15}$$

$$E_y = v_x B_z - v_z B_x + \eta J_y, \tag{16}$$

$$\mu_0 J_x = -\frac{\partial B_y}{\partial z}, \tag{17}$$

$$\mu_0 J_y = \frac{\partial B_x}{\partial z}. \tag{18}$$

Clearly B_z is a constant, which becomes a parameter of the problem. The solution of these equations also contains a free epicyclic oscillation of arbitrary amplitude and phase. That is, the equations are invariant under the transformation $v_x \mapsto v_x + 2a\sin[\Omega(t-\tau)]$, $v_y \mapsto v_y + a\cos[\Omega(t-\tau)]$, for any real numbers a and τ.[1] In general, the initial conditions will excite this motion at some amplitude.

In the limit of ideal MHD ($\nu = \nu_\mathrm{b} = \eta = 0$) the equations form a hyperbolic system, with wave speeds v given by

$$[(v-v_z)^2 - v_{\mathrm{a}z}^2][(v-v_z)^4 - (c_\mathrm{s}^2 + v_\mathrm{a}^2)(v-v_z)^2 + c_\mathrm{s}^2 v_{\mathrm{a}z}^2] = 0, \tag{19}$$

where $\boldsymbol{v}_\mathrm{a} = (\mu_0\rho)^{-1/2}\boldsymbol{B}$ is the Alfvén velocity. The six solutions are, of course, the Alfvén waves and the fast and slow magnetoacoustic waves.

If the upper boundary $z = Z$ is located above the slow magnetosonic point but below the Alfvén point, then two of the six waves are directed into the computational domain and the remaining four waves are directed outward. Therefore two boundary conditions should be applied to the six dependent variables $(v_x, v_y, v_z, \rho, B_x, B_y)$ there, and we do this by specifying the values of B_x and B_y, as discussed above.

4 WAVE SPEED LIMITER

A difficulty arises in solving the above system of equations if the density becomes very small above the disc. The very large Alfvén speed means that a very short timestep is required for stability unless an implicit integration scheme is adopted. It is possible to limit the wave speeds in a way that, to some extent, mimics the effects of Einsteinian relativity. This can be done by introducing a displacement current, replacing the definitions of J_x and J_y by

$$\mu_0 J_x + \frac{1}{c^2}\frac{\partial E_x}{\partial t} = -\frac{\partial B_y}{\partial z}, \tag{20}$$

$$\mu_0 J_y + \frac{1}{c^2}\frac{\partial E_y}{\partial t} = \frac{\partial B_x}{\partial z}, \tag{21}$$

[1] The electric field $\boldsymbol{E}$ undergoes a non-trivial transformation. In fact $\boldsymbol{E}$ is not the total electric field because it does not include the contribution (proportional to x) from induction by the Keplerian shear flow.

where c mimics the speed of light, but is a free parameter of the model. (Optionally, J_z and E_z can be included as well.) When $\nu = \nu_\mathrm{b} = \eta = 0$ we now have a hyperbolic system of equations. It is neither Galilean-invariant nor Lorentz-invariant, but this is convenient for our purposes because the added terms limit the speed of waves relative to the coordinate system (and the numerical grid) while having no effect on steady flows and their critical points. We use the wave speed limiter mainly as a convenient way of reaching steady solutions using fewer timesteps; these are then also steady solutions of the original problem. [The more complicated method of Miller & Stone (2000) does not appear to have this property, although it may have other desirable features.] In practice the wave speeds are limited to $\max(c, c_\mathrm{s} + |u_z|)$.

Provided that η is uniform, the system is still invariant under the addition of an epicyclic motion, although the transformation law of the electric field is modified.

5 QUASI-STEADY SOLUTIONS

5.1 ODE system

The system does not in fact admit truly steady solutions with an outflow unless a source of mass is included. In this case we obtain the system of ordinary differential equations (ODEs)

$$\rho\left(v_z\frac{\mathrm{d}v_x}{\mathrm{d}z} - 2\Omega v_y\right) = \frac{\mathrm{d}}{\mathrm{d}z}\left(\frac{B_x B_z}{\mu_0} + \rho\nu\frac{\mathrm{d}v_x}{\mathrm{d}z}\right), \tag{22}$$

$$\rho\left(v_z\frac{\mathrm{d}v_y}{\mathrm{d}z} + \frac{1}{2}\Omega v_x\right) = \frac{\mathrm{d}}{\mathrm{d}z}\left(\frac{B_y B_z}{\mu_0} + \rho\nu\frac{\mathrm{d}v_y}{\mathrm{d}z}\right), \tag{23}$$

$$\rho v_z\frac{\mathrm{d}v_z}{\mathrm{d}z} = -\rho\Omega^2 z + \frac{\mathrm{d}}{\mathrm{d}z}\left[-p - \frac{(B_x^2 + B_y^2)}{2\mu_0} + \rho(\nu_\mathrm{b} + \tfrac{4}{3}\nu)\frac{\mathrm{d}v_z}{\mathrm{d}z}\right], \tag{24}$$

$$\frac{\mathrm{d}}{\mathrm{d}z}(\rho v_z) = \dot\rho, \tag{25}$$

$$0 = \frac{\mathrm{d}}{\mathrm{d}z}\left(v_x B_z - v_z B_x + \eta\frac{\mathrm{d}B_x}{\mathrm{d}z}\right), \tag{26}$$

$$0 = -\frac{3}{2}\Omega B_x + \frac{\mathrm{d}}{\mathrm{d}z}\left(v_y B_z - v_z B_y + \eta\frac{\mathrm{d}B_y}{\mathrm{d}z}\right), \tag{27}$$

$$\frac{\mathrm{d}B_z}{\mathrm{d}z} = 0, \tag{28}$$

where $\dot\rho(z)$ is the mass source.

One possibility is to provide a mass source only on the midplane $z = 0$, so that $\dot\rho \propto \delta(z)$. The ODEs can then be solved in $z > 0$, with $\dot\rho = 0$. This procedure resembles the way in which steady accretion discs are treated without accounting for the (slow) increase in the mass of the central object. Alternatively, mass can be replenished at a rate proportional to the local density, so that $\dot\rho = \gamma\Omega\rho$, where γ is a small positive constant whose value can be adjusted to obtain a steady solution. In either case, mass is added to the solution at a rate that balances the outflow.

The solution is expected to be symmetrical about the

midplane, with ρ, v_x and v_y being even in z while v_z, B_x and B_y are odd. In the case of a mass source localized on the midplane, however, v_z is non-zero (and discontinuous) at $z = 0$.

The ideal MHD problem (in which $\nu = \nu_{\rm b} = \eta = 0$) has critical points wherever the wave speeds v given by equation (19) vanish. We assume that $\rho > 0$ and $v_z > 0$ for all $z > 0$. We expect that the flow will accelerate beyond the slow magnetosonic speed a few scale heights above the midplane, if the inclination of the poloidal field is appropriate. In a successful outflow the Alfvén and fast magnetosonic speeds will also be exceeded, but this will usually happen at a greater distance beyond the range of validity of the local approximation. We therefore consider only the slow magnetosonic critical point here.

We apply the following boundary conditions. At the top of the domain, $z = Z$, representing the 'surface' of the disc, we prescribe the values of B_x and B_y to be $B_{x\rm s}$ and $B_{y\rm s}$. The constant B_z is also given as an input parameter. The inclination angle i of the poloidal magnetic field is defined through $B_{x\rm s} = B_z \tan i$. At the midplane, $z = 0$, the symmetry conditions $B_x = B_y = 0$ apply, as well as $v_z = 0$ in the case of the distributed mass source. Finally, we require the surface density

$$2\int_0^Z \rho \,{\rm d}z = \Sigma \tag{29}$$

to equal a given value, which is one of the parameters of the model.

Of particular interest as an output of the calculation is the rate of mass loss per unit area from the upper surface of the disc,

$$\dot{m}_{\rm w} = \rho v_z\Big|_{z=Z}. \tag{30}$$

The timescale for depleting the mass of the disc is $\Sigma/(2\dot{m}_{\rm w})$.

Radial mass transport can also be induced in this model, despite the symmetries of the local approximation. Although the xy components of the viscous, Reynolds and Maxwell stresses are independent of x and therefore do not drive an accretion flow, the magnetic stress B_yB_z/μ_0 acting at the vertical boundaries can do so. In a steady state, the integrated azimuthal momentum equation (6) relates the radial transport velocity of mass, v_m, defined through

$$\Sigma v_m = \int_{-Z}^{Z} \rho v_x \,{\rm d}z, \tag{31}$$

to the yz stresses acting at $z = \pm Z$.

Furthermore, the radial transport velocity of poloidal magnetic flux, v_ψ, is given by

$$E_y = v_xB_z - v_zB_x + \eta\frac{\partial B_x}{\partial z} = v_\psi B_z. \tag{32}$$

The physical significance of this quantity is discussed by Ogilvie & Livio (2001) and Guilet & Ogilvie (MNRAS, submitted). It contains both an advective contribution, from motion in the meridional plane across the field lines, and a diffusive contribution.

Ogilvie & Livio (2001) solved a closely related problem for the vertical structure of magnetized discs with outflows. There are several differences. In that work, the problem was separated into an optically thick disc and an optically thin atmosphere. In the disc, the vertical velocity was neglected and the temperature was determined according to an energy equation including viscous and resistive heating and radiative diffusion. In the atmosphere, an isothermal outflow was computed along rigid magnetic field lines. Another difference is that the vertical transport of momentum by viscosity was neglected, while the radial transport of angular momentum was modelled in a way that goes beyond the standard local approximation.

5.2 Ideal MHD problem

We consider here the ideal MHD problem ($\nu = \nu_{\rm b} = \eta = 0$) with mass replenishment at the midplane. Assuming that the inclination of the poloidal magnetic field exceeds 30°, we expect to find a slow magnetosonic point at some height $z = z_{\rm s}$.

Given that $\dot{m}_{\rm w} = \rho v_z$ and $E_y = v_xB_z - v_zB_x$ are both independent of z, we can choose our vector of dependent variables to be

$$\boldsymbol{X} = \begin{bmatrix} v_y \\ v_z \\ B_x \\ B_y \end{bmatrix}. \tag{33}$$

The quantities ρ and v_x follow from the values of $\dot{m}_{\rm w}$ and E_y, which have the nature of eigenvalues, while B_z is a constant parameter. The remaining ODEs can be cast in the form

$$\mathbf{A}\frac{{\rm d}\boldsymbol{X}}{{\rm d}z} = \boldsymbol{Y}, \tag{34}$$

where

$$\mathbf{A} = \begin{bmatrix} 0 & B_xv_z & v_z^2 - v_{\rm az}^2 & 0 \\ v_z & 0 & 0 & -\frac{B_z}{\mu_0\rho} \\ 0 & v_z - \frac{c_{\rm s}^2}{v_z} & \frac{B_x}{\mu_0\rho} & \frac{B_y}{\mu_0\rho} \\ -B_z & B_y & 0 & v_z \end{bmatrix} \tag{35}$$

and

$$\boldsymbol{Y} = \begin{bmatrix} 2\Omega B_zv_y \\ -\frac{1}{2}\Omega v_x \\ -\Omega^2 z \\ -\frac{3}{2}\Omega B_x \end{bmatrix}. \tag{36}$$

At the slow magnetosonic point where

$$v_z = \left\{\frac{1}{2}(c_{\rm s}^2 + v_{\rm a}^2) - \left[\frac{1}{4}(c_{\rm s}^2 + v_{\rm a}^2)^2 - c_{\rm s}^2v_{\rm az}^2\right]^{1/2}\right\}^{1/2}, \tag{37}$$

the matrix $\mathbf{A}$ is singular. For a regular solution that passes smoothly through the slow point with finite derivatives, we require $\boldsymbol{L}\boldsymbol{Y} = 0$, where

$$\boldsymbol{L} = \begin{bmatrix} B_x & B_yB_z & B_z^2 - \mu_0\rho v_z^2 & B_yv_z \end{bmatrix} \tag{38}$$

is the null left eigenvector of $\mathbf{A}$ satisfying $\boldsymbol{L}\mathbf{A} = \mathbf{0}$ at this point. The regularity condition is therefore

$$B_yB_zv_x - 4B_xB_zv_y + 3B_xB_yv_z + 2\Omega z(B_z^2 - \mu_0\rho v_z^2) = 0. \tag{39}$$

A method of solution is as follows. The quantities $z_{\rm s}$ and E_y are guessed, as well as the values of B_x, B_y and ρ at the slow point. The value of v_z at the slow point follows by definition and hence the quantity $\dot{m}_{\rm w}$. The regularity condition determines the value of v_y. This is sufficient information to integrate the ODEs in each direction away from the slow

point. Away from the slow point and other critical points, the matrix $\mathbf{A}$ can be inverted to find $\mathrm{d}\boldsymbol{X}/\mathrm{d}z$ from $\boldsymbol{Y}$. We integrate down to $z = 0$ and require that $B_x = B_y = 0$ there. We also integrate up to $z = Z$ and require B_x and B_y to equal specified values there. A fifth condition is given by the mass integral (29). Using Newton–Raphson iteration, the five guessed quantities are adjusted to meet the five conditions.

This method fails if the Alfvén point is encountered below $z = Z$, because then the matrix $\mathbf{A}$ is singular and the solution cannot be made to pass smoothly through the critical point and match the specified values of B_x and B_y at $z = Z$.

A reduced version of the method is to assume that B_x and B_y have their limiting values already at the slow point. In that case no upward integration is required. There are only three quantities to guess and three conditions to be met.

5.3 Simplified version

A simplified version of the problem is obtained by neglecting v_x, v_z and B_y and solving the equations

$$-2\Omega v_y = \frac{B_z}{\mu_0\rho}\frac{\mathrm{d}B_x}{\mathrm{d}z}, \tag{40}$$

$$0 = -\Omega^2 z - \frac{1}{\rho}\frac{\mathrm{d}}{\mathrm{d}z}\left(p + \frac{B_x^2}{2\mu_0}\right), \tag{41}$$

$$0 = -\frac{3}{2}\Omega B_x + B_z\frac{\mathrm{d}v_y}{\mathrm{d}z}. \tag{42}$$

This procedure is equivalent to assuming an isorotational configuration with a purely poloidal magnetic field, as in Ogilvie (1997) and Ogilvie & Livio (1998) but with an isothermal gas. The boundary conditions are that B_x vanishes at $z = 0$ and has a specified value $B_z \tan i$ at large z, together with the constraint on the surface density.

Eliminating B_x, we obtain

$$\frac{\mathrm{d}}{\mathrm{d}z}\left(\frac{1}{2}\Omega^2 z^2 + c_\mathrm{s}^2 \ln\rho - \frac{2}{3}v_y^2\right) = 0 \tag{43}$$

and

$$B_z^2\frac{\partial^2 v_y}{\partial z^2} + 3\Omega^2\mu_0\rho v_y = 0. \tag{44}$$

For $i < 30^\circ$ there exist solutions for which $\rho \to 0$ and $B_x \to B_z \tan i$ as $z \to \infty$, while $v_y \sim (\frac{3}{2}\Omega\tan i)z + v_{y0}$, where v_{y0} is a constant. For large z this gives a declining density with $\ln\rho \sim -(1 - 3\tan^2 i)\Omega^2 z^2/2c_\mathrm{s}^2$. For $i > 30^\circ$, the gradient of v_y is sufficiently large that ρ would increase with z above a certain height, $z = [2\tan i/(3\tan^2 i - 1)](-v_{y0}/\Omega)$, and eventually B_x would be obliged to vary significantly. This indicates a breakdown of the static solution and the need for a transcritical outflow. The location of the minimum density gives a good indication of the location of the slow magnetosonic point in the corresponding solution with an outflow, and the rate of mass loss can be estimated from the static solution using a correction factor as in Ogilvie & Livio (1998).

This approximation is expected to be valid when the plasma beta at the slow point is small, i.e. $v_\mathrm{a}^2 \gg c_\mathrm{s}^2$. In this limit the condition for the slow point reduces to $v_z \approx c_\mathrm{s} v_{\mathrm{a}z}/v_\mathrm{a}$, and the regularity condition (39) reduces to

$$v_y \approx \frac{B_z\Omega z}{2B_x}, \tag{45}$$

which agrees with what is obtained by assuming an isorotational configuration and identifying the slow point as the location of the density minimum of the static approximation as described above.

5.4 Numerical simulation

In many ways it is easier to avoid the technical difficulties of directly computing steady solutions and instead to evolve the system forwards in time until a steady solution is approached, if it is stable. We use the wave speed limiter, usually with $c = 10c_\mathrm{s}$. A branch of steady solutions can be followed quasi-statically by slowing changing a parameter (such as B_z) during the simulation.

To integrate the equations we use tenth-order centred finite differences in z and a third-order explicit Runge–Kutta method in t. The method is usually stable when a version of the Courant condition on the timestep is satisfied. Boundary conditions are implemented with the help of ghost zones. In the case of the free 'outflow' boundary conditions on the velocity, the ghost zones are filled using linear extrapolation from the computational domain. If desired, mass replenishment can be carried out by either the localized or the distributed method.

6 NUMERICAL RESULTS

A dimensionless measure of the vertical magnetic field strength is

$$\frac{B_z}{\sqrt{\mu_0\Sigma c_\mathrm{s}\Omega}}. \tag{46}$$

Without loss of generality, we can choose units such that $\mu_0 = \Sigma = c_\mathrm{s} = \Omega = 1$. The remaining parameters are the three magnetic field components $(B_{x\mathrm{s}}, B_{y\mathrm{s}}, B_z)$ and the three diffusivities $(\nu, \nu_\mathrm{b}, \eta)$, whose values in these units can be interpreted as Shakura–Sunyaev alpha parameters.

We focus here on jet-launching solutions with $B_{x\mathrm{s}} = B_z$ and $B_{y\mathrm{s}} = 0$, for which the inclination of the poloidal magnetic field lines at the upper boundary is $i = 45^\circ$. The principal remaining parameter is the vertical magnetic field B_z. (The main effect of imposing a non-zero value of $B_{y\mathrm{s}}$ would be to apply a magnetic torque to the disc and thereby to drive a mean radial flow.)

We have computed quasi-steady solutions in ideal MHD as described in Section 5.2, using a Runge–Kutta method with adaptive stepsize. Mass is replenished at the midplane. Solutions are obtained for $B_z \gtrsim 0.7$; the height of the slow magnetosonic point and the rate of mass loss are plotted in Fig. 4. In these solutions the inclination of the poloidal magnetic field is fixed (i.e. $B_x = B_z$) at the slow point. For $B_z \gtrsim 1$ these quantities are accurately predicted by the simplified version of the problem described in Section 5.3. This behaviour is consistent with that found by Ogilvie (1997), Ogilvie & Livio (1998) and Ogilvie & Livio (2001). A stronger bending poloidal magnetic field produces a larger

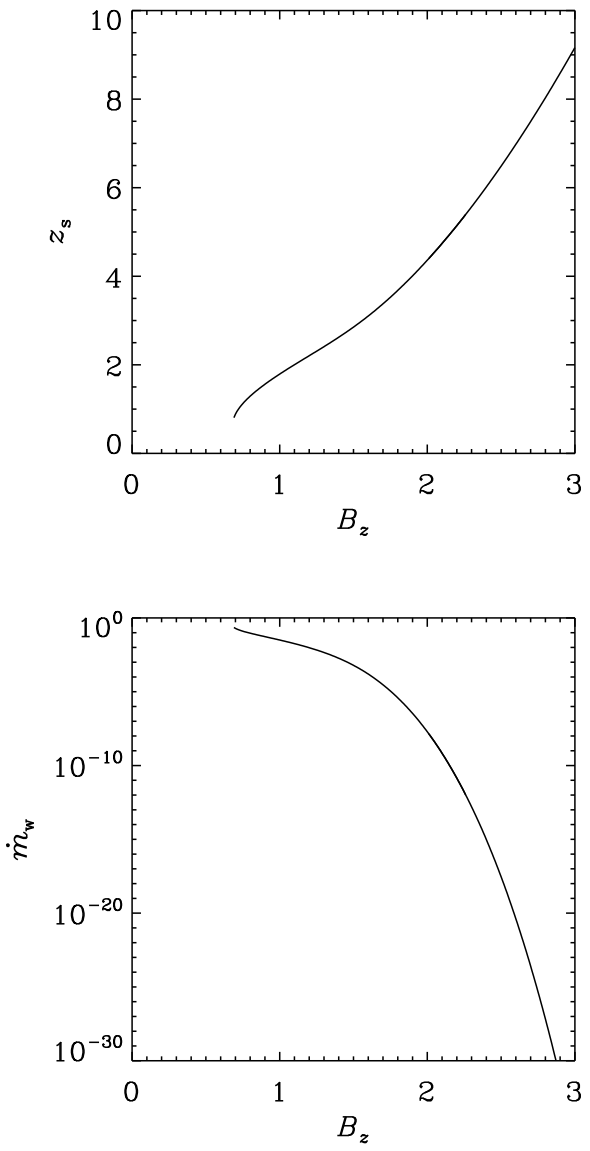

Figure 4. Top: Height of the slow magnetosonic point, in units of c_s/Ω, as a function of the vertical magnetic field strength, in units of $\sqrt{\mu_0 \Sigma c_s \Omega}$, for jet-launching solutions with inclination $i = 45°$. Bottom: One-sided mass-loss rate per unit area, in units of $\Sigma\Omega$.

radial Lorentz force, making the disc more sub-Keplerian (in the case of outward bending) and presenting a larger potential barrier to the outflow. The logarithm of the mass-loss rate is proportional to $-B_z^4$ at large B_z. In practice, the outflow is completely suppressed when the dimensionless magnetic field strength increases by a factor of only 2 or 3. However, the maximum value of $\dot{m}_w$ plotted in Fig. 4 is about 0.23, which corresponds to the disc being emptied on a time-scale of approximately 0.35 orbits!

We have also carried out numerical simulations in non-ideal MHD as described in Section 5.4. In a typical numerical simulation we solve the equations in the domain $-5 < z < 5$ with 1000 grid points and with diffusivities $\nu = \nu_b = \eta = 0.03$. A clean start can be obtained by initializing the simulation with the quasi-steady solution up to the slow magnetosonic point. It is straightforward in this way to obtain strongly magnetized solutions, e.g. at $B_z = 2$. In this regime the poloidal magnetic field does straighten well before $z = 5$, and a steady outflow is achieved, with a rate of mass loss that is insensitive to the location of the boundary. With a less careful initial condition, a permanent epicyclic oscillation is generally obtained on top of the quasi-steady solution, while other wave modes damp slowly through viscosity and resistivity. The epicyclic oscillation can be avoided only by initializing the horizontal momentum correctly, but its presence has no effect on the jet-launching process.

The presence of non-zero diffusivities slightly reduces the rate of mass loss. As an example, for $B_z = 2$, diffusivities of 0.03 reduce the mass loss by about 7% compared to the ideal-MHD solution.

The value of B_z can be decreased slowly and continuously during the simulation, or the simulation can be restarted periodically with slightly smaller values of B_z. As this is done, the height of the slow point decreases and the rate of mass loss increases dramatically. Eventually the system becomes unstable to the MRI. If the simulation maintains perfect symmetry about the midplane, then the first MRI mode to be observed is expected to be similarly symmetric; if an antisymmetric seed perturbation is introduced, then an antisymmetric MRI mode is expected to set in first. In practice it is difficult to observe a clean development of the MRI with such an inclined poloidal field. The mass loss is so strong in this regime that either the disc empties very quickly or the details of the replenishment process become important; depending on how momentum is treated in this process, a rapid artificial growth of epicyclic motion may occur. This transitional regime is also problematic because the density of the outflow is so large that the Alfvén point and fast magnetosonic point approach the disc and the interpretation of the solutions becomes unclear; there is no longer a force-free region of straight field lines in which the inclination of the field can be meaningfully imposed.

Without mass replenishment, the surface density decreases in time, with the effect that the disc becomes more strongly magnetized: the value of $B_z/\sqrt{\mu_0 \Sigma c_s \Omega}$ increases. If this parameter starts close to 1, then rapid mass loss occurs and the parameter increases quickly until the mass loss abates. In this way a burst of ejection occurs. In a global model of a disc, this condition might be met at different times at different radii, leading to a 'wave' of ejection.

7 CONCLUSION

The acceleration of an outflow along inclined magnetic field lines emanating from an accretion disc can be studied in the local approximation, as employed in the shearing-box model. By imposing the inclination of the magnetic field at the vertical boundaries of the box and resolving the slow magnetosonic point within the computational domain, appropriate solutions with outflows can be obtained and the rate of mass loss can be calculated.

This procedure works best when the magnetic field is sufficiently strong to suppress the magnetorotational instability (MRI). As found in previous work, in this regime the

mass-loss rate is extremely sensitive to the dimensionless field strength $B_z/\sqrt{\mu_0\Sigma c_{\rm s}\Omega}$, allowing the possibility of an explosive burst of ejection from any radius in the disc at which the appropriate field strength is attained.

It would be of interest to determine the stability of these solutions with respect to perturbations that depend on x and/or y, to test for the instabilities discussed by Lubow & Spruit (1995) and Lubow, Papaloizou & Pringle (1994). For weaker fields it may be possible to study the jet launching process in parallel with the MRI. While that is a much more demanding problem, the present paper may provide some useful guidance.

ACKNOWLEDGMENTS

This research was supported by STFC. I am grateful to Xuening Bai, Sébastien Fromang, Jérôme Guilet, Geoffroy Lesur and Jim Stone for useful discussions.

REFERENCES

Balbus S. A., Hawley J. F., 1998, RvMP, 70, 1
Blandford R. D., Payne D. G., 1982, MNRAS, 199, 883
Goldreich P., Lynden-Bell D., 1965, MNRAS, 130, 125
Hawley J. F., Gammie C. F., Balbus S. A., 1995, ApJ, 440, 742
Lubow S. H., Spruit H. C., 1995, ApJ, 445, 337
Lubow S. H., Papaloizou J. C. B., Pringle J. E., 1994, MNRAS, 268, 1010
Miller K. A., Stone J. M., 2000, ApJ, 534, 398
Ogilvie G. I., 1997, MNRAS, 288, 63
Ogilvie G. I., Livio M., 1998, ApJ, 499, 329
Ogilvie G. I., Livio M., 2001, ApJ, 553, 158
Spruit H. C., 1996, in Wijers R. A. M. J., Davies M. B., Tout C. A., eds, Evolutionary Processes in Binary Stars, Kluwer, Dordrecht, 249
Suzuki T. K., Inutsuka S., 2009, ApJ, 691, L49
Suzuki T. K., Muto T., Inutsuka S., 2010, ApJ, 718, 1289